Halpern, M. S., and Koshland, M. E. (1970), *Nature (London) 228,* 1276.
Halpern, M. S., and Koshland, M. E. (1973), *J. Immunol. 111,* 1653.
Mestecky, J., and Schrohenloher, R. E. (1974), *Nature (London) 249,* 650.
Mestecky, J., Schrohenloher, R. E., Kulhavy, R., Wright, G. P., and Tomana, M. (1974), *Proc. Natl. Acad. Sci. U.S.A. 71,* 544.
Metzger, H. (1970), *Adv. Immunol. 12,* 57.
Munn, E. A., Feinstein, A., and Munro, A. J. (1971), *Nature (London) 231,* 527.
Prahl, J. W., Abel, C. A., and Grey, H. M. (1971), *Biochemistry 10,* 1808.
Putnam, F. W., Florent, G., Paul, C., Shinoda, T., and Shimizu, A. (1973), *Science 182,* 287.
Reisfeld, R. A., and Small, P. A. (1966), *Science 152,* 1253.
Smith, W. L., and Ballou, C. E. (1974), *Biochem. Biophys. Res. Commun. 59,* 314.
Wilde, C. E. III, and Koshland, M. E. (1973), *Biochemistry 12,* 3218.
Wolfenstein-Todel, C., Mendez, E., Prelli, F., Frangione, B., and Franklin, E. C. (1974), in The Immunoglobulin A System, Mestecky, J., and Lawton, A. R., Ed., New York, N.Y., Plenum Publishing Co., p 257.

Shape and Volume of Fragments Fab′ and $(Fab')_2$ of Anti-Poly(D-alanyl) Antibodies in the Presence and Absence of Tetra-D-alanine as Determined by Small-Angle X-Ray Scattering†

Ingrid Pilz, Otto Kratky, Arieh Licht, and Michael Sela*

ABSTRACT: The conformation of two fragments derived from anti-poly(D-alanyl) antibodies, the divalent fragment $(Fab')_2$ and the monovalent fragment Fab′, was studied by small-angle X-ray scattering before and after interaction with the tetra-D-alanine amide hapten. More than 90% of the combining sites were occupied by the hapten. No significant changes were observed in the volume or in the radius of gyration, with either of the fragments. This contrasts with the significant decrease in these two parameters found upon reacting the hapten with intact anti-poly(D-alanyl) antibodies (I. Pilz, O. Kratky, A. Licht, and M. Sela (1973), *Biochemistry 12,* 4998). For Fab′, the radius of the whole particle was found to be 3.48 nm in the absence of the hapten and 3.46 nm in its presence, the radius of gyration of the cross-section was 1.37 nm without hapten and 1.38 nm in its presence, and the volume of the particle was 92 nm^3 in the absence of the hapten and 91 nm^3 in its presence. For $(Fab')_2$ the respective values were 5.06 and 5.05, 1.38 and 1.37, and 182 and 182. These results suggest that a conformational change occurs within the antibody molecule, but not within its Fab fragment, upon reaction with the tetraalanine hapten.

In a recent study (Pilz et al., 1973b) by small-angle X-ray scattering of anti-poly(D-alanyl) antibodies, a significant volume contraction could be observed upon interaction with the tetra-D-alanine hapten. The anti-poly(D-alanyl) antibodies obtained by immunization with poly(D-alanyl) diphtheria toxoid showed a decrease of the volume by 10% and a decrease of the radius of gyration by 7.7% when 90% of the binding sites were occupied by hapten. Qualitatively similar results were obtained when intact antibodies of a different specificity (anti-*p*-azophenyl β-lactoside) were reacted with the homologous hapten (Pilz et al., 1973a).

In view of these results it was of interest to find out whether the interaction of the hapten with fragments derived from an intact antibody, and still possessing active combining sites, would be also accompanied by changes in radius of gyration and in volume. For this purpose, we have prepared from anti-poly(D-alanyl) antibodies by peptic digestion the divalent fragment $(Fab')_2$. From this divalent fragment we prepared by reduction and alkylation the monovalent fragment Fab′. Both Fab′ and $(Fab')_2$ were reacted with tetra-D-alanine amide, and their volumes and radii of gyration were determined by small-angle X-ray scattering, before and after the interaction with the hapten. The results show clearly that the radius of gyration and the volume of each one of the two antibody fragments studied did not change significantly as a result of the interaction with the tetrapeptide.

Materials and Methods

The preparation of the antigen poly(D-alanyl) diphtheria toxoid has been previously described (Licht et al., 1971). It contained 20 D-alanine residues attached per protein molecule, distributed with the average of 2.8 chains, containing 7.1 D-alanine residues/chain. Preparation of the ligands

† From the Institute for Physical Chemistry, University of Graz, Graz, Austria (I.P.), Institut für Röntgenfeinstrukturforschung, Graz, Austria (O.K.), and Department of Chemical Immunology, The Weizmann Institute of Science, Rehovot, Israel (A.L. and M.S.). *Received September 27, 1974.* This study was supported in part by the "Österreichischen Fonds zur Förderung der wissenschaftlichen Forschung," by Grant 06-010 from the National Institutes of Health, U.S. Public Health Service, Bethesda, Md., and Grant No. 280 of the United States-Israel Binational Science Foundation.

tetra-D-alanine amide and the radioactive peptide (D-Ala)$_3$-[^{14}C]Gly was described elsewhere (Schechter, 1971).

Immunization. Rabbits were immunized with the antigen poly(D-alanyl) diphtheria toxoid. Three 1-ml successive doses of 10 mg/ml of antigen in complete Freund's adjuvant were injected intramuscularly, at 10- and 30-day intervals, respectively. Sera were collected after the second injection, at 1-week intervals. Specific anti-poly(D-alanyl) antibodies were isolated by means of the water-insoluble poly(D-alanyl) rabbit serum albumin-cellulose immunoadsorbent, as described previously (Licht et al., 1971). The experiments were performed on pooled antibodies from different animals.

Fragmentation of IgG Antibodies. The (Fab')$_2$ fragment was prepared by pepsin digestion of the IgG molecules (10 mg/ml) in 0.1 *N* sodium acetate buffer (pH 4.5) by a modification of the method of Nisonoff et al. (1960). Pepsin 1:50 (w/w) was added to the antibody solution. The solution was incubated for 16 hr at 37°. The (Fab')$_2$ fragment was then purified by gel filtration on Sephadex G-150 in 0.01 *M* sodium phosphate–0.15 *M* sodium chloride (pH 7.4). The Fab' fragment was prepared from the (Fab')$_2$ fragment by reduction for 1 hr with 0.01 *M* dithiothreitol in 0.1 *M* Tris buffer (pH 8.2) at room temperature. The reduction was followed by alkylation with 4.5 mg/ml of iodoacetamide, and dialysis after 30 min against 0.01 *M* sodium phosphate–0.15 *M* sodium chloride (pH 7.4). Characterization of the protein fractions was done by immunodiffusion and immunoelectrophoresis experiments, using anti-Fc and anti-Fab antibodies. Concentrations of the protein solutions were determined from their nitrogen content found by Kjeldahl analysis. The extinctions $E_{1cm}^{1\%}$ obtained were 14 for the Fab' fragment and 14.5 for the (Fab')$_2$ fragment.

Preparation of Fragment Samples for Small-Angle X-Ray Scattering. The preparations of both fragments Fab' and (Fab')$_2$ were divided into two portions. One of them was equilibrated by dialysis with a buffer solution of 0.01 *M* sodium phosphate–0.15 *M* sodium chloride (pH 7.4) and remained free of hapten, whereas the other was equilibrated with the same buffer but including also 1×10^{-3} *M* (D-alanyl)$_3$-D-alaninamide; under these conditions both fragments were saturated with hapten. Ligand occupancy of the fractions was determined by equilibrium dialysis using the radioactive tetrapeptide (D-Ala)$_3$-[^{14}C]Gly as hapten, and found to be above 90%. Concentration series (5–50 mg/ml) were measured for all preparations.

Small-Angle X-Ray Scattering Measurements. The small-angle measurements were done with a highly stabilized X-ray generator (Philips PW 1140), using a copper tube. A camera (Kratky, 1958) with slit collimation was used. The experimental curves, therefore, include the collimation effect; they are slit smeared. This is indicated by a tilde (e.g., $\tilde{I}$, $\tilde{R}$), whereby $\tilde{I}$ means the slit-smeared intensity and $\tilde{R}$ the value of the apparent radius of gyration, calculated directly from the experimentally obtained, slit smeared scattering curves. The collimation effects, caused by the line shape of the primary beam, were eliminated by a computer program described by Glatter (1974).

The solutions of the fragments were placed in Mark capillaries (diameter about 0.1 cm) and irradiated at a temperature of 5°. The scattered intensities were recorded using a proportional counter with pulse-height discriminator as a detector for the Cu lines Kα and Kβ. Elimination of the Kβ line was effected using a computer program (Zipper, 1969).

An electronically programmable step scanning device

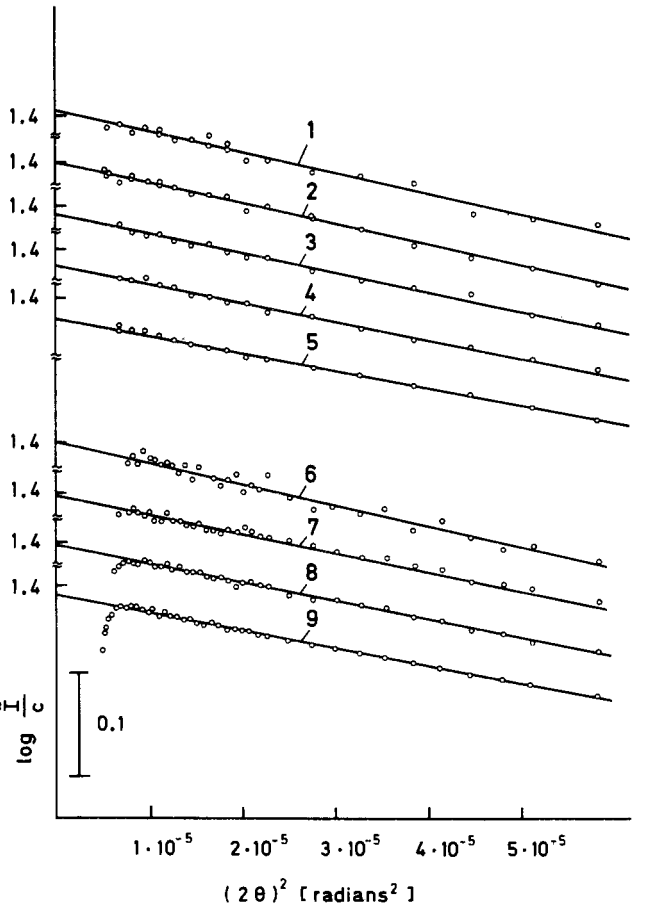

FIGURE 1: Innermost portions of the slit-smeared scattering curves of anti-poly(D-alanyl) fragment Fab' in solution in a Guinier plot. The concentration (c) of the fragments in solution and the apparent radii of gyration ($\tilde{R}$) calculated from the slope of the straight lines are summarized in Table I; the numbers in the figure correspond to the numbers in the table; $\tilde{I}$ = slit-smeared scattered intensity; 2θ = scattering angle.

(Kratky and Kratky, 1964; Leopold, 1965) combined with the X-ray measuring equipment of Philips allowed automatic operation. The scattered intensities were measured at 65 different scattering angles in a range between 0.0021 and 0.1 radian; an entrance slit of 120 μm was used. Each single solution was exposed to X-rays for about 12 hr. During this period its scattering curve was recorded several times, whereby as a rule 2×10^4 pulses were registered for each measuring point. The evaluation of the scattering data was done by using a computer program of Zipper (1972). Since no alteration in the scattering behavior was detected during exposure to X-rays, conformation changes due to radiation damage could be excluded.

Theory. From the small-angle X-ray scattering curves the following data were calculated: radius of gyration R, radius of gyration of the cross-section R_q, and volume V of the antibody fragments in solution, by using the invariant (Porod, 1951). Further models equivalent in scattering were calculated with a computer program (O. Glatter, in preparation). The equations used for these calculations have already been given in this journal (Pilz et al., 1970). Summarizing papers about these methods are those of Kratky (1963), Kratky and Pilz (1972), and Pilz (1973).

Results

Radius of Gyration. The apparent radii of gyration $\tilde{R}$ were calculated from the slope of the innermost portions of

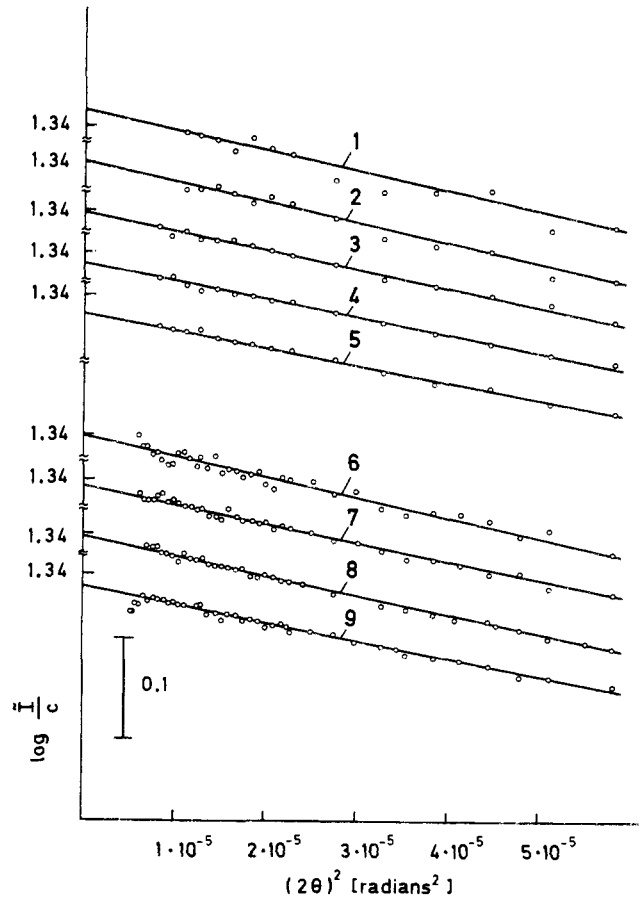

FIGURE 2: Innermost portions of the slit-smeared scattering curves of anti-poly(D-alanyl) fragment Fab′ after interaction with hapten; above 90% of the combining sites of the fragment are occupied by hapten. The concentrations (c) of the solutions and the apparent radii of gyration ($\tilde{R}$), calculated from the slopes of the straight lines, are summarized in Table I; the numbers in the figure correspond to the numbers in the table. $\tilde{I}$ = slit-smeared scattered intensity, 2θ = scattering angle.

Table I: Apparent Radii of Gyration $\tilde{R}$ Calculated from the Slopes of the Guinier Straight Lines of Figures 1 and 2 (Free and Bound Fragment Fab′) and Figures 4 and 5 (Free and Found Fragment $(Fab')_2$).[a]

Fab′					
Free			Saturated with Hapten (above 90%)		
No. in Fig. 1	c (mg/ml)	$\tilde{R}$ (nm)	No. in Fig. 2	c (mg/ml)	$\tilde{R}$ (nm)
1	5.64	2.91	1	6.42	2.88
2	11.3	2.87	2	10.4	2.86
3	20.9	2.81	3	21.3	2.80
4	33.1	2.73	4	34.5	2.72
5	49.5	2.64	5	49.5	2.64
6	5.59	2.90	6	9.81	2.87
7	20.1	2.81	7	21.5	2.80
8	29.9	2.76	8	28.9	2.76
9	49.5	2.65	9	49.5	2.65
$(Fab')_2$					
Free			Saturated with Hapten (above 90%)		
No. in Fig. 4	c (mg/ml)	$\tilde{R}$ (nm)	No. in Fig. 5	c (mg/ml)	$\tilde{R}$ (nm)
1	10.5	4.11	1	5.08	4.12
2	22.3	4.04	2	10.2	4.10
3	36.0	3.95	3	20.2	4.05
4	49.5	3.94	4	30.5	4.02
			5	49.5	3.92
			6	6.25	4.14
			7	9.83	4.11
			8	18.5	4.03
			9	29.5	4.06
			10	49.5	3.93

[a] c is the concentration of the fragments in solution.

the scattering curves in the Guinier plot as shown in Figures 1 and 2.

Fragment Fab′. Figure 1 gives the experimental scattering curves of two series of measurements of the anti-poly(D-alanyl) fragment Fab′ free of hapten, and Figure 2 gives two series of curves of the same fragment in which practically all combining sites were occupied by the hapten. The apparent radii of gyration $\tilde{R}$ calculated from the slope of the straight lines shown in Figures 1 and 2 are summarized in Table I. In Figure 3a the $\tilde{R}$ values obtained are plotted vs. the corresponding concentrations of the fragments in solution. It is seen that the $\tilde{R}$ values of the Fab′ fragment free of hapten, and those of the same fragment saturated with hapten, are identical within the error of measurement.

Fragment $(Fab')_2$. Figures 4 and 5 show the analogous curves for the anti-poly(D-alanyl) fragment $(Fab')_2$. In Figure 4 are given the curves for the fragment free of hapten. In Figure 5 are shown the curves for the situation in which practically all combining sites were occupied by the hapten. In Figure 3b the apparent radii of gyration $\tilde{R}$ calculated from Figures 4 and 5 are plotted vs. the concentration of the fragment. The $\tilde{R}$ values of the $(Fab')_2$ fragment free and saturated with hapten are also identical within the errors of measurement.

Up to now only the unsmoothed experimentally obtained scattering data are given, because they show clearly the errors of measurement and the fact that changes in the conformation of the fragments upon the binding of hapten, if any, cause no change in the $\tilde{R}$ value within these errors of measurement (compare Figure 3 and Table I).

The correct values of the radii of gyration after elimination of the collimation effect and extrapolation to zero concentration (see Figure 3) are given for all fragments free and saturated with hapten in Table II.

Radius of Gyration of the Cross-Section. The cross-section curves of the four different samples (free and bound fragments Fab′ and $(Fab')_2$) are shown in Guinier plot in Figure 6. The radii of gyration of the cross-section R_q calculated from the straight-line part of the curves are very similar. All values are about 1.4 nm, and correspond to the flat outermost portion of the cross-section curves of the whole IgG molecule (Pilz et al., 1970; Pilz et al., 1973b). The R_q values are summarized in Table II for the more concentrated solutions only, since the scattering curves of the diluted solutions show larger statistical errors in these outer parts of the scattering curves from which the data of the cross-section can be calculated. The small differences in the R_q values (Table II) are within the experimental errors, since the R_q values can be determined with less accuracy than the R values of the whole particle.

Only very long particles have cross-section curves in which there is a straight-line course in the Guinier plot also at very small angles. The cross-section curves of particles, the length of which is only several times their diameter, differ from the cross-section curves of very long particles by their low intensities at very small angles. The angles at which the Guinier plots deviate from straight lines become

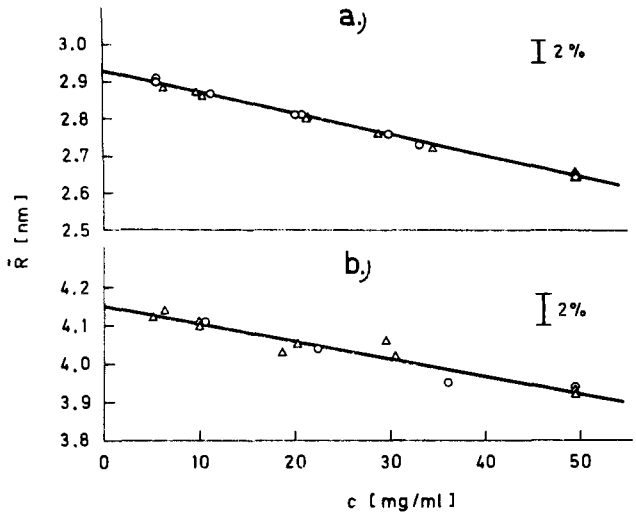

FIGURE 3: Apparent radii of gyration ($\tilde{R}$) plotted vs. the concentration (c) of the fragments in solution. (a) (○) Values of the free fragments Fab′; (△) values of the Fab′ having above 90% of the active sites occupied by hapten; (b) (○) values of the free fragments $(Fab')_2$; (△) values of the $(Fab')_2$ having above 90% of the active sites occupied by hapten.

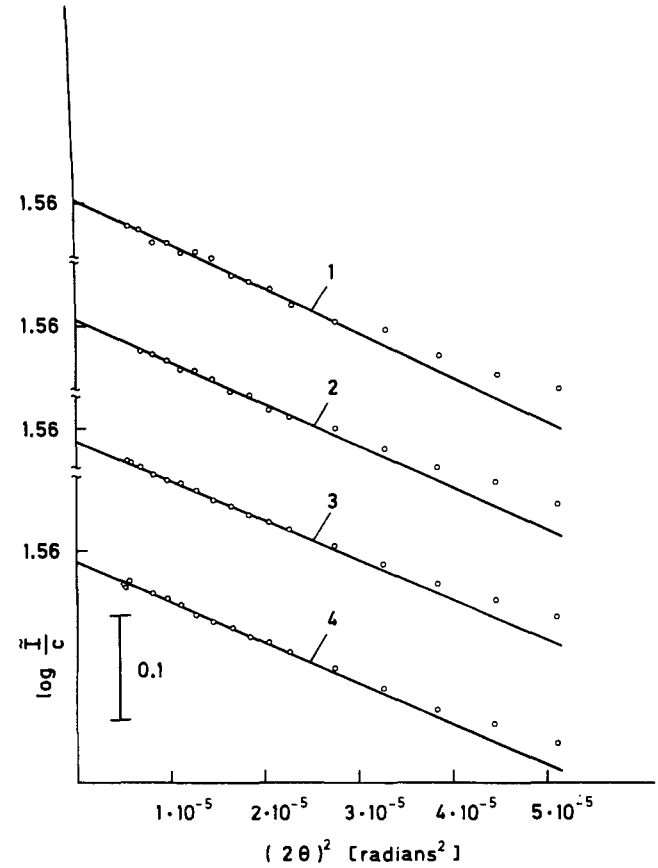

FIGURE 4: Innermost portions of the slit-smeared scattering curves of anti-poly(D-alanyl) fragments $(Fab')_2$ in solution in Guinier plot. The concentration (c) of the fragments in solution and the apparent radii of gyration ($\tilde{R}$) calculated from the slopes of the straight lines are summarized in Table I; the numbers in the figure correspond to the numbers in the table; $\tilde{I}$ = slit-smeared scattered intensity; 2θ = scattering angle.

larger, as the length of the particle becomes smaller in comparison to its diameter. Since the curve of the Fab′ fragment deviates at correspondingly larger angles from the Guinier straight line (see Figure 6), it can be concluded immediately that this fragment must be shorter than the $(Fab')_2$ fragment. The ratio 2:1 for length to diameter of a particle is the lower limit at which it is possible to find in a relatively small angle range a straight-line course and to determine from its slope the R_q value. Pilz et al. (1970) used successfully as an approximation a model assuming that the Fab fragment resembles a cylinder. According to this model the Fab′ fragment is only twice as long as its diameter, and therefore the straight-line course is much less pronounced than with the longer $(Fab')_2$ fragment. It should be pointed out also that a cross-section can be determined not only for rigid elongated particles, but also for bent elongated particles.

Volume. The volumes of the different particles were determined using Porod's invariant (1951). The value of the invariant Q, whereby $Q = \int_0^\infty I(2\theta)^2 d(2\theta)$, was calculated in the following way: in an angle range of 0–0.08 radian, the integration was performed using the Simpson rule. At larger angles the scattering curves showed a course oscillating around $k/(2\theta)^4$ and in the angle range 0.08–∞ the integration was performed analytically after determining the value of the constant k. It should be pointed out that the volumes determined in this way correspond to the hydrated particles including also small voids. The absolute accuracy of the determination of the volume is not very high by this method, but the relative accuracy, i.e., the comparison of the volumes of similar particles in similar buffers (as in the present case) under identical conditions, is much better; the relative volumes can be determined with an error of 1–2%.

The volumes for the different preparations are listed in Table II. It is seen that the volumes of the Fab′, free and saturated with hapten, are identical within the error of measurement. The volumes of the $(Fab')_2$, free and saturated with hapten, are also identical and have twice the value found for Fab′. No change of the volume is associated with the occupancy of the combining sites of the fragments with hapten within the error of measurement.

Since the concentration of the solutions could not be determined with sufficient accuracy, the molecular weights and partial specific volumes of the fragments could not be calculated exactly. Assuming average values of mol wt 50,000 for the Fab′ and mol wt 100,000 for the $(Fab')_2$, and an average partial specific volume of 0.733, the following values for the unhydrated volumes V_{unh} of the fragments can be calculated: V_{unh} = 61 nm³ for the Fab′ and V_{unh} = 121 nm³ for the $(Fab')_2$. Comparing these unhydrated volumes of the protein mass of the fragments with the experimentally found hydrated volumes of the fragments (see Table II), for both fragments a degree of hydration of 0.36 g of H_2O/1 g of protein is found.

Shape. The data mentioned up to now as radii of gyration, volume, and molecular weight can be calculated from the scattering of the particle without making further assumptions. The relation between the shape of the particle and the form of its scattering curve is not immediately apparent, since the variety of colloid structures is very great. However, it is possible to get information about the overall shape of the particle and to find a model which is equivalent in scattering, for instance, by comparing the experimental scattering curve with the theoretically calculated scattering curves of various models.

As a first approximation usually simple triaxial bodies of

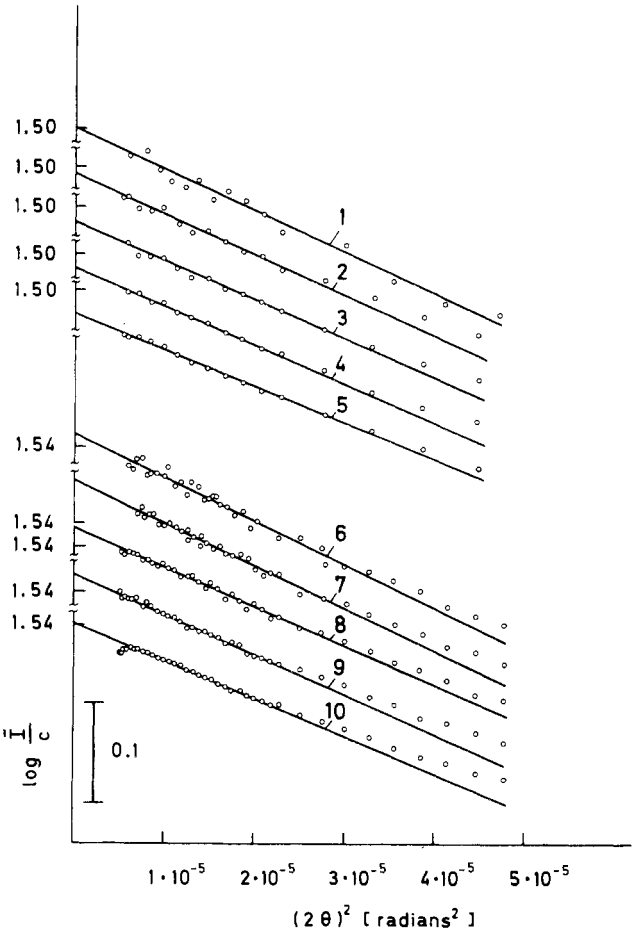

FIGURE 5: Innermost portions of the slit-smeared scattering curves of anti-poly(D-alanyl) fragments $(Fab')_2$ after interaction with hapten; above 90% of the binding sites are occupied by hapten. The concentration (c) of the fragments in solution and the apparent radii of gyration ($\tilde{R}$) are summarized in Table I; the numbers in the figure correspond to the numbers in the table; $\tilde{I}$ = slit-smeared scattered intensity; 2θ = scattering angle.

Table II: Data for Fragments Fab' and $(Fab')_2$.[a]

	R (nm)	R_q (nm)	V (nm³)
Fab'			
Free	3.48	1.37	92
Above 90% saturation	3.46	1.38	91
$(Fab')_2$			
Free	5.06	1.38	182
Above 90% saturation	5.05	1.37	182[a]

[a] Fragments Fab' and $(Fab')_2$ are free or have above 90% of the combining sites occupied by hapten. V = volume of the particle. R = radius of gyration of the particle, R_q = radius of gyration of the cross-section.

uniform electron density are used as models. The dimensions of such a model equivalent in scattering can be calculated using the experimental value of the radius of gyration. If the particle under investigation possesses, according to the approximation made, a nearly uniform electron density, the correct dimensions of the overall shape may be found. For particles whose electron density distribution deviates essentially from a uniform one, e.g., for particles having clefts and regions of low density inside, too large dimensions are found if a uniform electron density is assumed. This follows immediately from the definition of the radius of gyration, which increases for a particle possessing constant volume with the anisotropy and hollowness. With highly symmetric isotropic particles, which have a number of pronounced subsidiary maxima, it can be deduced from the height of these maxima that there is a hollow space inside (Pilz et al., 1970). With particles of lower symmetry and isotropy, such as the fragments Fab' and $(Fab')_2$ it is not possible to deduce clefts or regions of lower density, which are placed inside the particle. Since the X-ray crystallographic studies on Fab (Poljak et al., 1973) show that the fragment has a centrally located cleft, not only models of uniform electron density but also models corresponding to the X-ray crystallographic shape were calculated.

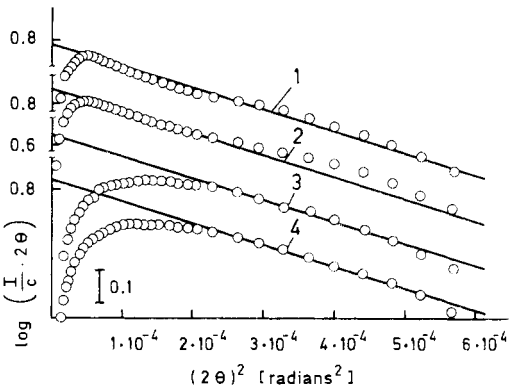

FIGURE 6: Cross-section curves in Guinier plot of the following anti-poly(D-alanyl) fragments in solution: curve 1, $(Fab')_2$, above 90% of the binding sites occupied by hapten, concentration (c) of the fragment = 30.5 mg/ml, curve 2, free $(Fab')_2$, c = 49.5 mg/ml; curve 3, Fab', above 90% of the binding sites occupied by hapten, c = 49.5 mg/ml; curve 4, free Fab', c = 49.5 mg/ml; I = scattered intensity, 2θ = scattering angle. The radii of gyration of the cross-section R_0 calculated from the slopes of the straight lines are given in Table II.

Fab'. In Figure 7 are shown the experimental scattering curves of the free fragment (curve 1) and of the fragment saturated to the extent of above 90% with hapten (curve 2). The curves are very similar: small differences revealed only in the angle region of the first subsidiary maximum. Chosing simple triaxial bodies of uniform electron density as models, an elliptical cylinder (semiaxis 2.1 nm and 1.8 nm, height 11 nm, curve 3) shows best similarity, but the agreement is not satisfactory. Much better agreement is obtained with models which possess a cleft inside. Curve 4 is the scattering curve of the model A shown in Figure 8. This model, built up of a number of spheres, corresponds to a first approximation to the X-ray crystallographic model of Poljak et al., 1973. The shape of this model fits the form of the experimental curve better, but its radius of gyration is 2.96 nm, clearly lower than the experimentally found value of 3.4 nm; further the volume of all spheres constructing the model is lower than the experimental value found for the hydrated molecule in solution. To obtain a model the radius of gyration and volume (sum of the volumes of the spheres) of which would fit the experimental data model A was increased by adding further spheres and increasing the central cavity (model B). The scattering curve of this model B (curve 5) fits the experimental curve well at low angles, and shows also a shoulder at the same position as the experimental curves. It should be pointed out that the information obtained by small-angle scattering is of course not sufficient to prove this model with certainty; it is only a possible model which fits well the data found for the molecule in solution.

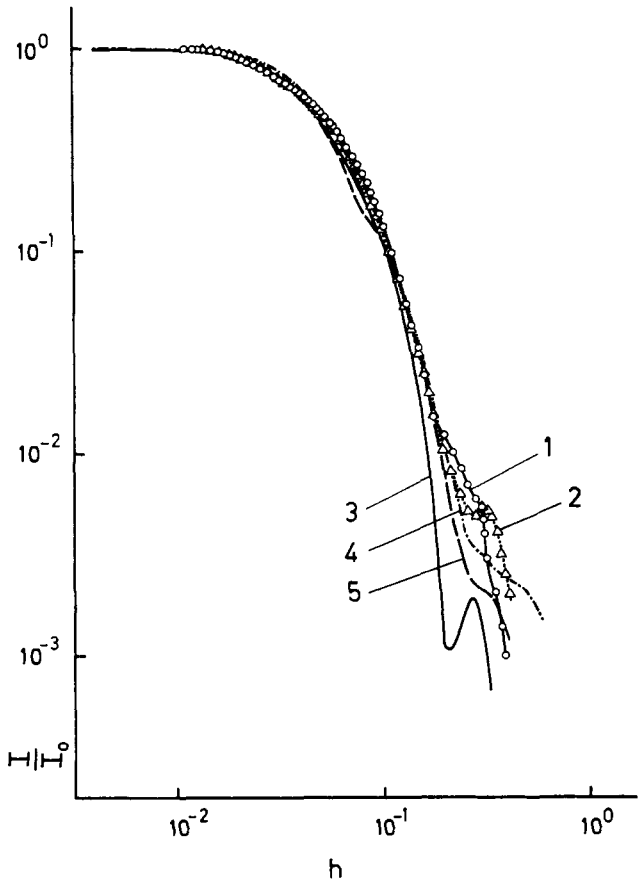

FIGURE 7: Comparison of the experimental scattering curves of the fragment Fab′ with theoretical curves of various models in log–log plot: curve 1 (O—O), experimental curve of the free fragment Fab′, R = 3.48 nm; curve 2 (Δ—Δ), experimental curve of Fab′ after interaction with hapten (above 90% saturation); R = 3.46 nm; curve 3 (—) calculated curve of an elliptical cylinder of uniform electron density (height = 11.1 nm, semiaxes = 2.1 nm and 1.8 nm, radius of gyration R = 3.49 nm); curve 4 (---), scattering curve of model A in Figure 8 (R = 2.96 nm); curve 5 (——), scattering curve of model B in Figure 8 (R = 3.4 nm). I = scattered intensity, I_0 = scattered intensity at zero angle, $h = (4\pi/\lambda)$ in θ, where θ is half the scattering angle and λ the wavelength (0.154 nm).

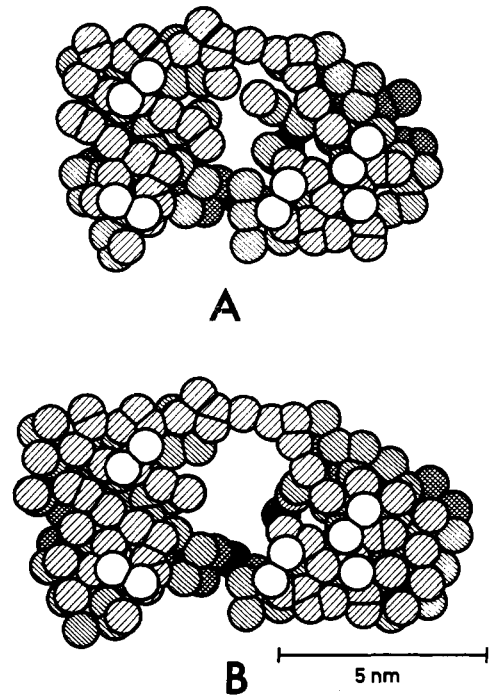

FIGURE 8: Two models composed of spheres the radius of which is 0.44 nm. Model A corresponds in its dimensions to the X-ray crystallographic model of Poljak et al. (1973); it has the same cleft inside and its radius of gyration is 2.96 nm. Model B is deduced from model A by adding some spheres and increasing the central cavity to obtain a model the radius of gyration of which corresponds to the experimental one of R = 3.4 nm and the volume of its spheres to the experimentally found hydrated volume.

$(Fab')_2$. In Figure 9 are shown the experimental scattering curves of the free fragment (curve 1) and of the fragment saturated with hapten (curve 2). The curves are very similar; only at larger angles, where the small shoulder appears, are there any differences.

Comparison of the experimental curves of the $(Fab')_2$ fragment with the curves of various models showed clearly that the two Fab′ fragments cannot be connected in the direction of the longest axes to a completely stretched particle which has twice the length of the single Fab′ fragment. Only models in which the two Fab′ fragments are arranged at an angle (model 3 and 4 in Figure 9) fit the experimental curve at small angles. At larger angles, however, the scattering curves of model 3 and 4, with which a uniform electron density without clefts inside is assumed, deviate from the experimental curve. A much better agreement is obtained by arranging not two homogeneous cylinders as shown in model 4 (Figure 9) but two models B (see Figure 8) at an angle (curve 5, Figure 9).

Discussion

The main result of the investigation of fragments, derived from anti-poly(D-alanyl) antibodies, in the presence and absence of the hapten tetra-D-alanine amide, is that the occupancy of the specific sites caused no change in their volume and in their radius of gyration. This should be contrasted with the occupancy of the specific binding sites of the intact antibody molecules by haptens, which caused a significant change both in the radius of gyration and in the volume of the antibodies (Pilz et al., 1973a,b).

The radius of gyration and volume of both fragments remained unchanged within the error of measurement, although above 90% of the binding sites of the fragments were saturated with hapten. Only at the outer part of the scattering curve, where a small subsidiary maximum appears, are there some small differences. Thus, the free fragments Fab′ and $(Fab')_2$ show only a small shoulder in this region, whereas a maximum (for Fab′) and a pronounced shoulder (for $(Fab')_2$) can be observed after saturation with hapten (Figures 7 and 9).

These results indicate that the occupancy of the specific binding sites of the fragments by the haptens caused no change in the overall shape, and that only very small changes of the conformation are possible. This agrees very well with the recent crystallographic data, showing no significant change within the Fab′ molecule upon binding a specific ligand (Padlan et al., 1973; Amzel et al., 1974). The values obtained for the Fab′ fragment (volume, radius of gyration, and radius of gyration of the cross-section, Table II) are similar to those found earlier for the Fab fragment of a γG1 immunoglobulin (Pilz et al., 1970).

As already mentioned (Pilz et al., 1973a), the shape found for the intact antibodies agrees with that obtained by Sarma et al. (1971) from crystal X-ray studies. On the other hand, considerable differences in the dimensions of

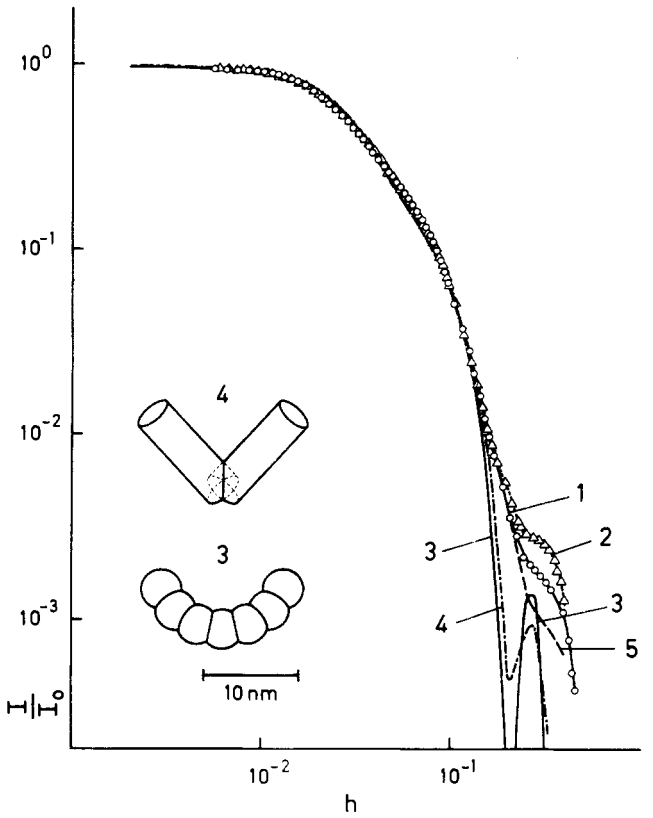

FIGURE 9: Comparison of the experimental scattering curve of the fragment $(Fab')_2$ with theoretical curves of various models in log–log plot: curve 1 (O—O), experimental curve of free $(Fab')_2$ (R = 5.06 nm); curve 2 (Δ—Δ), experimental curve of $(Fab')_2$ after interaction with hapten (above 90% saturation, R = 5.05 nm); curve 3 (—), theoretical curve of the model 3 shown in the figure (R = 5.1 nm); curve 4 (---), theoretical curve of the model 4 shown in the figure (R = 5.07 nm); curve 5 (——) theoretical curve of a model composed of two models B (compare Figure 8) arranged at an angle similar to model 3 (R = 5.07 nm). Detailed description of the models in the text. I = scattered intensity, I_0 = scattered intensity at zero angle, $h = (4\pi/\lambda)\sin\theta$, whereby θ is half the scattering angle and λ the wavelength (0.154 nm).

the molecule were persistently found. A model of uniform electron density, which is equivalent in scattering with the small-angle data, is much more extended than the X-ray crystallographic model.

The same effect was found for the Fab′ fragment. The dimensions obtained for the Fab′ fragment using a simple model of uniform electron density are considerably larger than those found by Poljak et al. (1973) by X-ray crystallographic studies. The overall dimensions of the crystallographic model are 8.0 × 5.0 × 4.0 nm, whereas those of a model of uniform electron density equivalent with the small-angle data are 11 × 4.2 × 3.6 nm. The difference in the dimensions is lowered very much if the model of uniform electron density is replaced with a model having a cleft inside analogous to the model of Poljak et al. Such a model fits all the small angle data better—especially the form of the scattering curve—and has the smaller dimensions of 9 × 5 × 4 nm (caused by the cleft inside as discussed under "shape").

Thus, the main discrepancy in the dimensions disappears if models of nonuniform electron density, with hollow spaces inside, are used. But, in spite of this fact, the Fab′ fragment seems to be more extended in solution, since the model of Poljak et al. (1973) has a radius of gyration of only about 3.0 nm, clearly lower than the experimentally found one of 3.4 nm. The largest dimension of the X-ray crystallographic model would have to increase from 8 to 9 nm, to fit the small angle data. Whether this is partly caused by an ion or water cloud shell, or whether the fragment is really more extended in solution, cannot be decided.

In agreement with earlier investigations on an $(Fab')_2$ fragment of γG1 immunoglobulin, it was found that the Fab′ regions are not connected end to end in the direction of the longest axis. The radius of gyration of such a structure is considerably higher for a model of uniform electron density (R = 6.6 nm), and also higher for a model composed of two models B (see Figure 8) connected end to end in a stretched way (R = 6.0 nm). Models which fit the experimental R value are only obtained if the two Fab′ fragments are arranged at an angle to each other. Two models of this type are seen in Figure 9. In model 3 the $(Fab')_2$ fragment is approximated by a number of spheres (diameter 4.4 nm), in model 4 by two elliptic cylinders each representing one Fab fragment (height 11 nm, semiaxes 2.1 nm and 1.8 nm). Both models have the same radius of gyration as experimentally found (R = 5 nm), but deviate at large angles from the experimental scattering curve (Figure 9). A better agreement is found if two models B (Figure 8) are arranged at an angle. The calculated scattering curve of this model fits the experimental curves best, as seen in Figure 9.

If the contraction of the volume of the antibody molecule upon reaction with the hapten would be due to changes within the area of the combining site, it would be expected that these changes would persist in antibody fragments, which still possess fully active combining sites. Our findings, that no such changes can be observed in the fragments, leads to the conclusion that the decrease in the volume and in the radius of gyration of the intact antibody molecule is due to conformative changes affecting large portions of the molecule, and assigns a definite role to the Fc fragment of the molecule, and/or the hinge region, possibly affecting the spatial relationship of the two Fab fragments. In agreement with our conclusion about conformational changes within the antibody in areas remote from the combining site, Givol et al. (1974) reported recently that, as a consequence of antigen binding, conformational changes occur in both the Fab and the Fc fragments of the antibody. They followed the changes by measuring the circular polarization of luminescence.

It might be suggested, as an additional explanation of our results, that the native antibody—in contrast to the fragments—is self-associating in solution, and that the addition of hapten lowers the protein–protein interaction. In this case the decrease in volume and in the radius of gyration of the complete antibody upon reaction with tetra-D-alanine would be due to prevention of self-association, rather than contraction of molecules. Even if this explanation would be valid, it would still lead to the conclusion that a change had to occur in the conformation of the Fc fragment, which is the obvious candidate for the self-association.

It is predicted on the basis of our conclusions that—in contrast to the lack of easily detectable changes within the Fab fragment upon binding a ligand, as followed by X-ray diffraction techniques—crystals of intact antibody should exhibit distinct changes upon reaction with hapten or antigen.

Acknowledgments

The gift of tetra-D-alanine peptides from Dr. Israel Schechter is gratefully acknowledged. I.P. thanks Miss

Karin Walder for excellent technical assistance and Mrs. Erika Schwarz and Miss Božena Müller for valuable experimental help.

References

Amzel, L. M., Poljak, R. J., Saul, F., Varga, J. M., and Richards, F. F. (1974), *Proc. Natl. Acad. Sci. U.S.A. 71,* 1427.

Givol, D., Pecht, I., Hochman, J., Schlessinger, J., and Steinberg, I. Z. (1974), in Progress in Immunology, Vol. 1, Brent, L., and Holbrow, J., Ed., Amsterdam, North-Holland Publishing Co., p 39.

Glatter, O. (1974), *J. Appl. Crystallogr. 7,* 147.

Glatter, O. (in preparation).

Kratky, O. (1958), *Z. Elektrochem. 62,* 66.

Kratky, O. (1963), *Prog. Biophys. 13,* 105.

Kratky, C., and Kratky, O. (1964), *Z. Instrumentenkd. 72,* 302.

Kratky, O., and Pilz, I. (1972), *Q. Rev. Biophys. 5,* 481.

Leopold, H. (1965), *Elektronik 14,* 359.

Licht, A., Schechter, B., and Sela, M. (1971), *Eur. J. Immunol. 1,* 351.

Nisonoff, A., Wissler, F. C., Lipman, L. N., and Woernley, D. L. (1960), *Arch. Biochem. Biophys. 89,* 230.

Padlan, E. A., Segal, D. M., Spande, T. F., Davies, D. R., Rudikoff, S., and Potter, M. (1973), *Nature (London), New Biol. 245,* 165.

Pilz, I. (1973), in Physical Principles and Techniques of Protein Chemistry, Part C, Leach, S. J., Ed., New York, N.Y., Academic Press, p 141.

Pilz, I., Kratky, O., and Karush, F. (1973a), *Eur. J. Biochem. 41,* 91.

Pilz, I., Kratky, O., Licht, A., and Sela, M., (1973b), *Biochemistry 12,* 4998.

Pilz, I., Kratky, O., and Moring-Claesson, I. (1970), *Z. Naturforsch., Teil B 25,* 600.

Pilz, I., Puchwein, G., Kratky, O., Herbst, M., Haager, O., Gall, W. E., and Edelman, G. M. (1970), *Biochemistry 9,* 211.

Poljak, R. J. Amzel, L. M., Avey, H. P., Chen, B. L., Phizackerley, R. P., and Saul, F. (1973), *Proc. Natl. Acad. Sci. U.S.A. 70,* 3305.

Porod, G. (1951), *Kolloid-Z. 124,* 83.

Sarma, R., Silverton, E. W., Davies, D. R., and Terry, W. D. (1971), *J. Biol. Chem. 246,* 3753.

Schechter, I. (1971), *Ann. N.Y. Acad. Sci. 190,* 394.

Zipper, P. (1969), *Acta Phys. Austriaca 30,* 143.

Zipper, P. (1972), *Acta Phys. Austriaca 36,* 27.